Biomedical Optics EXPRESS

Bimodal spectroscopy for *in vivo* characterization of hypertrophic skin tissue : pre-clinical experimentation, data selection and classification

H. Liu,[1] **H. Gisquet,**[2]**, W. Blondel,**[1] **and F. Guillemin,**[3]

[1]*Université de Lorraine 2, avenue de la forêt de Haye, Nancy, 54516, France*
[2]*Centre Hospitalier Universitaire de Nancy, 29 Avenue du Maréchal de Lattre de Tassigny, Nancy, 54000, France*
[3]*Centre Alexis Vautrin, 6 avenue de bourgogne, Vandoeuvre-les-Nancy, 54511, France*
**liuhonghui@msn.com*

Abstract: This study aims at investigating the efficiency of bimodal spectroscopy in detection of hypertrophic scar tissue on a preclinical model. Fluorescence and Diffuse Reflectance spectra were collected from 55 scars deliberately created on ears of 20 rabbits, amongst which some received tacrolimus injection to provide non-hypertrophic scar tissue. The spectroscopic data measured on hypertrophic and non-hypertrophic scar tissues were used for developing our classification algorithm. Spectral features were extracted from corrected data and analyzed to classify the scar tissues into hypertrophic or non-hypertrophic. The Algorithm was developed using k-NN classifier and validated by comparing to histological classification result with Leave-One-Out cross validation. Bimodal spectroscopy showed promising results in detecting hypertrophic tissue (sensibility 90.5%, specificity 94.4%). The features used for classification were extracted from the autofluorescence spectra collected at 4 CEFS with excitations at $360,410 and 420 nm$. This indicates the hypertrophic process may involve change in concentration of several fluorophores (collagen, elastin and NADH) excited in this range, or modification in volume of explored tissue layers (epidermis and dermis) due to tissue thickening .

OCIS codes: (120.6200) Spectrometers and spectroscopic instrumentation ; (300.6550) Spectroscopy, visible ; (070.4790) Spectrum analysis.

Références

1. V. Zatsiorsky and W. Kraemer, *Science and practice of strength training*, 2nd ed. (Human Kinetics, 2006).
2. B. Berman and W. Valins and S. Amini and M.H. Viera, "Keloid and hypertrophic scar," http ://emedicine.medscape.com/article/1057599-overview.
3. C. W. Kischer and G. S. Brody, "Structure of the collagen nodule from hypertrophic scars and keloids," Scan. Electron. Microsc. **3,** , 371–376 (1981).
4. G. A. Wagnieres, W. M. Star, and B.C. Wilson, "In vivo fluorescence spectroscopy and imaging for oncological applications," Photochem Photobiol. **5,** 603–632 (1998).
5. K. Koenig and H. Schneckenburger, "Laser-induced autofluorescence for medical diagnosis," J. Fluorescence. **4,** 17–40 (1994).
6. I. Georgakoudi, J. Motz, V. Backman, G. Angheloiu, and A. Haka, "Quantitative characterization of biological tissue using optical spectroscopy," in Biomedical Photonics Handbook, V.-D. Tuan, ed. (CRC Press, 2003), pp. 1–27.

#171682 - $15.00 USD Received 29 Jun 2012; revised 27 Sep 2012; accepted 28 Sep 2012; pub. 16 Nov 2012

7. R. R. Anderson and J. A. Parrish, "The optics of fuman skin,' J. Investigat. Dermatol. **77,** 13–19 (1981).
8. I. Georgakoudi, B.C. Jacobson, and J.V. Dam, "Fluorescence, reflectance, and light-scattering spectroscopy for evaluating dysplasia in patients with Barret's esophagus,' Gastroenterology **120**(7), 1620–1629 (2001).
9. I. Georgakoudi, E. E. Sheets, M. G. Müller, and V. Backman, "Trimodal spectroscopy for the detection and characterization of cervical precancers *in vivo*,' Am. J. Obstetr. Gynecol. **186**(3), 374–382 (2002).
10. N. Ramanujam, "Fluorescence spectroscopy of neoplastic and non-neoplastic tissues,' Neoplasia **2**(1-2), 89–117 (2000).
11. N. M. Marìn, A. Milbourne, and H. Rhodes, "Diffuse reflectance patterns in cervical spectroscopy,' Gynecol. Oncol. **99**(3), 116–120 (2005).
12. S.M. Chidananda, K. Satyamoorthy, and L. Rai, "Optical diagnosis of cervical cancer by fluorescence spectroscopy technique,' Int. J. Cancer **119**(1), 139–145 (2006).
13. R. J. Nordstrom, L. Burke, J. M. Niloff, and J. F. Myrtle, "Indentification of cervical intraepithelial neoplasia(CIN) using UV-excited fluorescence and diffuse-reflectance tissue spectroscopy,' Lasers Surg. Med. **29,** 118–127(2001).
14. C. Zhu, G.M. Palmer, and T.M. Breslin, "Use of a multisepartation fiber optical probe for the optical diagnosis of breast cancer,' J. Biomed. Opt. **10**(2), 024032 (2001).
15. J. R. Mourant, I. J. Bigio and J. Boyer, "Spectroscopic diagnosis of bladder cancer with elastic light scattering,' Lasers Surg. Med. **17,** 350–357 (1995).
16. B. W. Murphy and R. J. Webster, "Toward the disctrimination of early melanoma from common and dysplastic nevus using fiber optic diffuse reflectance spectroscopy,' J. Biomed. Opt. **10**(6), 064020 (2005).
17. G. Zonios, L.T. Perelman, and V. Backman, "Diffuse reflectance spectroscopy of human ademonatous colon polyps,' Appl. Opt. **38**(31), 6628–3667 (1999).
18. E. Pery, W. C. P. M. Blondel, J. Didelon, and F. Guillemin, "Simultaneous characterization of optical and rheological properties of carotid arteries via bimodal spectroscopy : experimental and simulation results' IEEE Trans. Biomed. Eng. **56**(5), 1267–1276 (2009).
19. G. Diaz-Ayil, M. Amouroux, W. C. P. M. Blondel, G. Bourg-Heckly, Y. Granjon, and F. Guillemin, "In vivo diagnosis of mouse skin precancerous stages using autofluorescence and diffuse reflectance bimodal spectroscopy : instrumentation, spectral feature extraction and linear classification,' Appl. Phys. **47,** 012707 (2009).
20. M. Amouroux, G. Diaz-Ayil, W. C. P. M. Blondel, G. Bourg-Heckly, A. Leroux, and F. Guillemin, "Classification of ultra-violet irradiated mouse skin histological stages by bimodal spectroscopy (multiple excitation autofluorescence and diffuse reflectance),' J. Biomed. Opt. **14**(1), 014011 (2009).
21. G. Chen, J. Chen, S. Zhuo, S. Xiong, H. Zeng, X. Jiang, R. Chen, and S. Xie, "Nonlinear spectral imaging of human hypertrophic scar based on two-photon excited fluorescence and second-harmonic generation,' Br. J. Dermotol. **161,** 48–55 (2009).
22. N. M. Marin, N. McKinnon, and C. MacAulay, "Calibration standards for multicenter clinical trial of fluorescence spectroscopy for *in vivo* diagnosis' J. Biomed. Opt. **11**(1), 014010 (2006).
23. H. Gisquet, H. Liu, W. C. P. M. Blondel, A. Leroux, F. Guillemin, J. L. Merlin, D. Peiffert, and C. Latarch, "Intradermal Tacrolimus prevent scar hypertrophy in a rabbit ear model. A clinical, histological and spectroscopical analysis,' Skin Res. Technol. **17**(2), 160–166 (2011).
24. J. E Jackson, *User's guide to Principle Component* (Wiley, 1991).
25. M. Dash and H. Liu, "Features selection for classification' Intell. Data Anal. **1**, 131–156 (1997).
26. M. Schumacher, N. Hollander, and W. Sauerbrei, "Resampling and cross-validation techniques : a tool to reduce bias caused by model building,' Stat. Med. **16**(24), 2813—2827 (1997).
27. K. Sokolov, J. Galvan, A. Myakov, A. Lacy, R. Lotan, and R. Richards-Kortum, "Realistic three-dimensional epithelial tissue phantoms for biomedical optics,' J. Biomed. Opt. **7**(1), 148—156 (2002).
28. J. A. Palero, H. S. de Bruijn, A. van der Ploeg-van den Heuvel, H. J. C. M. Sterenborg, and H. C. Gerritsen, "In vivo nonlinear spectral imaging in mouse skin,' Opt. Express **14**(10), 4395–4402 (2006).
29. G. N. Stamatas, R. B. Estanislao, M. Suero, Z. S. Rivera, J. Li, A. Khaiat, and N. Kollias, "Facial skin fluorescence as a marker of the skin's response to chronic environmental insults and its dependence on age,' Opt. Express **154**(1), 125–132 (2006).
30. R. Benninger, O. Hofmann, J. McGinty, J. Requejo-Isidro, I. Munro, M. Neil, A. de Mello, and P. French, "Time-resolved fluorescence imaging of solvent interactions in microfluidic devices,' Opt. Express **13**(16), 6275–6285 (2005).
31. A. Pena, M. Strupler, T. Boulesteix, M. Schanne-Klein, "Spectroscopic analysis of keratin endogenous signal for skin multiphoton microscopy,' Opt. Express **13**(16), 46268–46274 (2005).
32. N. Kollias, G. Zonios, and G. N. Stamatas, "Fluorescence spectroscopy of skin,' Vibrat. Spectrosc. **28,** 17–23 (2002).
33. K. M. Katika and L. Pilon, "Steady-state directional diffuse reflectance and fluorescence of human skin,' Appl. Opt. **45**(17), 4174—4183 (2006).
34. F. Koenig, R. Larne, H. Enquist, F. J. McGovern, K. T. Schomacker, N. Kollias, and T. F. Deutsch, "Spectroscopic measurement of diffuse reflectance for enhanced detection of bladder carcinoma,' J. Urol., **51**(2), 342–345 (1998).

#171682 - $15.00 USD Received 29 Jun 2012; revised 27 Sep 2012; accepted 28 Sep 2012; pub. 16 Nov 2012

35. V. Tuchin, *Tissue Optics : Light Scattering Methods and Instruments for Medical Diagnosis* (SPIE, 2007).
36. O. Kloeters, A. Tandara, and T. A. Mustoe, "Hypertrophic scar model in the rabbit ear : a reproducible model for studying scar tissue behavior with new observations on silicone gel sheeting for scar reduction' Wound Repair Regenerat. **15**(Suppl. 1), S40–S45(2008).
37. R. Kortum and E. Muraca, "Quantitative optical spectroscopy for tissue diagnosis,' Annu. Rev. Phys. Chem. **47,** 555–606 (1996).

1. Introduction

Hypertrophy is defined as an increase in tissular volume of an organ, resulting from normal physiological process [1] or caused by abnormal accumulation of tissular components, such as hypertrophic scars or keloids occurred on human skin. In the latter case, the excessive growth of the scar can be of great cosmetic concern when occurring on the face, or result in functional loss of nearby organs [2]. Hypertrophic scars occurring in all age groups has higher incidence rate for individuals aged 10-20. They are common in African subjects following a traumatic event on skin. In some people, keloid may recur spontaneously after treatment.

Cutaneous hypertrophic scars are due to an accumulation of collagen cross-links (accounting for tissue hardening) and to an overproduction of collagen, raising above the surrounding skin or growing indefinitely beyond the boundaries of the original wound into a large, tumorous (although benign) neoplasm. Kischer and Brody [3] identified collagen nodules to be the structural unit of hypertrophic scars and keloids. These nodules, which are absent from mature scars, contain higher density of fibroblasts and unidirectional collagen fibrils in a highly organized and distinct orientation. In addition, hypertrophic scars differ from normal skin by the presence of richer vasculature (depending on scar age), higher mesenchymal cell density, and thickened epidermal cell layer. Keloidal scars, depending on their maturity, are mainly composed of either type III (early) or type I (late) collagen.

At present, clinical examination is the major method for hypertrophic scar tissue diagnosis. But, involving biopsy and subsequent histological analysis, it is of poor sensitivity and time-consuming [2]. Removal of the suspected scar tissue, leading to higher skin tension, would prolong the wound's healing and raise the risk of hypertrophy incidence. Thus, a non-invasive method for characterizing this kind of tissue *in vivo* is of prior interest for both clinicians and patients.

In the frame of developing non invasive diagnostic methods for *in vivo* tissue characterization, fibred optical spectroscopy has been widely studied over the last several decades [4–6]. In contrast to surgical biopsy, the spectroscopic methods don't require any tissue removal. The principle consists in exploiting tissue-light interactions between near-UV and near-infrared (NIR) to probe the optical properties of the biological tissues *in vivo*. The main interactions exploited are absorption, scattering and fluorescence [7]. The resulting intensity spectra are measured and serve for developing classification algorithms to automatically characterize the tissue states [8–10].

Light Induced Fluorescence Spectroscopy (LIFS) is one of the most studied spectroscopic methods for characterizing pathological tissues in cervix [11–13], esophagus [8], breast [14] and skin [19]. Biochemical and structural modifications associated to disease development can involve significant changes in intra-cellular and extra-cellular constituents among which some fluoresce under proper light excitation. These endogenous fluorophores include amino acids (tryptophan and tyrosine), structural proteins (collagen and elastin), pyridine nucleotides (NADH and NADPH), flavins and porphyrins. The AutoFluorescence (AF) emitted by these molecules is modulated by various factors, such as tissular concentration, quantum yield or biochemical environment. When pathological phenomena occur, these modulating factors are modified and change the bulk fluorescence intensity emitted by the tissue. Spatially resolved Diffuse Reflectance (DR) spectroscopy is another fibred optic technique efficiently applied in

#171682 - $15.00 USD Received 29 Jun 2012; revised 27 Sep 2012; accepted 28 Sep 2012; pub. 16 Nov 2012

tissue photodiagnosis *in vivo* [11, 15, 16]. It consists in measuring the light backscattered by the tissue after multiple scattering and absorption of photons from an incident light over a wide wavelength band (350-750nm). The spectral features of the DR spectra depend on the scattering and absorbing properties of the tissue, involving main chromophores such as hemoglobin, melanin and water. A number of studies have demonstrated that the latter could change significantly for different tissue conditions [15, 17]. So, a diagnosis algorithm could be created by exploiting the optical-property-based spectroscopic features. The tissue depths to which the optical properties can be analyzed are determined by the multiple fiber probe geometry, as well as the excitation wavelength(s) [14]. Several fibers with different Collecting-to-Exciting Fiber separation (CEFS) are used for providing various probing depths, but with a limitation to the superficial layers of the tissue especially for UV-Visible wavelengths (a few hundreds of micrometers). Furthermore, numerous studies [8, 18–20] showed that each of these techniques separately provides complementary information on the tissue status, but that combining both (bimodal configuration) can bring superior diagnostic results.

As skin hypertrophy in scar tissues introduces a series of morphological and structural changes involving several fluorophores and chromophores (namely collagen, elastin, hemoglobin), we applied bimodal (multiple AF and DR) spectroscopy to diagnose hypertrophic scar tissues on a preclinical model. An anti-inflammatory drug, whose inhibition effect of hypertrophy formation had been tested along with this study, was partially applied to the model. We obtained not only hypertrophic but also non-hypertrophic scar tissues for spectra measurement. An experimental protocol was strictly followed for ensuring high quality data acquisition. Specific algorithms were developed for classifying each tissue site automatically based on discriminant spectroscopic features. The efficiency of the method was asserted upon sensibility and specificity obtained by comparing the classification results with those from histological analysis.

2. Materials and Methods

2.1. Pre-clinical model

Up to the present, rabbit's ear is the only animal model that provides reproducible hypertrophic scar for *in vivo* study [36]. Hence, the protocol described in [36] was applied on 20 rabbits' ears to induce hypertrophic scar for our study. All procedures followed the Helsinki rules and were approved by the animal regional ethic committee of Northeastern France (january 2009). In brief (please refer to [23] for details), 20 New Zealand female white rabbits, between 2.5 and 4 kg and aged about 100 days (CEGAV, Les Hautes Noes, France), were kept under standard condition and fed *ad libitum* for 2 weeks before the experiment. Then, they were anesthetized by intramuscular injection of ketamine ($45 mg/kg$) and xylazine ($7 mg/kg$). The ventral surface of rabbits' ear was shaved and treated with chlorhexidine to avoid wound's infection. Two $10 mm$-diameter wounds were created on each ear with help of a circular dye cutter by removing the underneath perichondrium down to bare cartilage. The wounds were spaced from each other by 4 cm in order to avoid inter-wound reaction. They had been covered by Tegaderm dressing (Tegaderm, 3M Health Care, St.Paul, MN) until entirely re-epithelialized. Hypertrophic scars appeared basically in 28 days after the initial wounding. An immunomodulator drug with anti-inflammatory and antifibrinogenic proliferation properties (Tacrolimus), whose efficiency on inhibiting hypertrophic scar formation was investigated in [23], was applied to certain wounding in order to create non-hypertrophic scar tissues for comparison.

2.2. Spectroscopy instrumentation and measurement protocol

The spatially resolved bimodal spectroscopic system used in the present work was adapted from the one developed by [19,20]. In brief (see Fig. 1), it consists of an infrared-filtered $300 W$

#171682 - $15.00 USD Received 29 Jun 2012; revised 27 Sep 2012; accepted 28 Sep 2012; pub. 16 Nov 2012

Xenon arc lamp (PE30-BF PerkinElmer, Eurosep, France) producing excitation light in the range of 350-750*nm*. The lamp's output light is focused by a plano-convex lens on the entrance of a bunch of seven optical fibers (individual core diameter $200\mu m$, numerical aperture 0.22) grouped together in a unique SMA connector. Between the light source and the SMA entrance, band-pass excitation filters (mounted on a filter wheel) and a couple of linearly variable short- and long-pass filters (LVF-series Linear Variable Filters, Ocean Optics) are used to configure the spectral shape of the excitation light for our experimental requirement. The positioning of all these filters is automated by linear or rotative motorized stages (LTA Long-Travel actuators and M-UMR8.51 linear stages, Newport) which are controlled by a dedicated motion controller (XPS motion controller, Newport). The use of this motion controller allow us programmable multi-excitation measurements. For DR measurements, a wide band excitation ($350-750nm$) is required. In our experimental set-up, an extra linear motorized stage (Newport) was used during DR measurements to extend the travel distance of the LVFs so as to free the light path between the lens and the excitation fiber entrance.

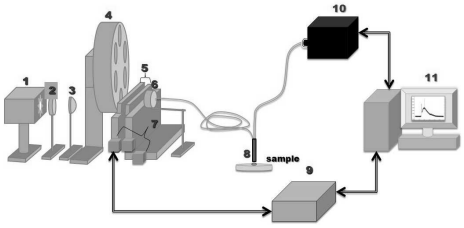

FIG. 1. Schematics of the spatially resolved bimodal fibred spectroscopy set up. 1) Short arc Xenon Source 2) Heat control filter 3) Plano condenser lens 4) Wide band-pass filter wheel 5) Combined set of short- and long-pass linearly variable filters 6) Excitation fiber positioning stage 7) Micrometric translation stages 8) Fiber optics probe (distal tip) 9) Micrometric stage motor controller 10) Imaging Spectrograph 11) PC computer

In order to explore various tissue depths, 6 fibers were chosen to collect the light re-emitted by tissue at the 6 following CEFS : 429, 438, 453, 672, 696 and $1090\mu m$. These collecting fibers are connected inline to the entrance slit of a multi-channel spectrometric system (iHR320 Imaging spectrometer, Symphony STE CCD, Jobin Yvon, HORIBA®). This system acquires the intensity spectra coming simultaneously from the 6 collecting fibers, allowing for spatially resolved measurements. The spectrometer features a diffraction grating groove of $150gr/nm$ density, which span the largest measure range ($496nm$) in keeping a relatively high spectral resolution ($1.2nm$). The spectrograph also features an internal filter wheel with 4 different long-pass filters alternatively used to eliminate the back-reflected excitation light from detection during AF measurements (see Table 1). For the present study, 9 narrow intensity peaks (FWHM$= 15 \pm 2nm$) ranging from 360 to $450nm$ by step of $10nm$ were chosen for AF measurement, and a wide wavelength range $350-700nm$ was used for DR measurement (cf. 1). The latter were automatically configured by loading a preset configuration file. A multi-excitation measurement on one tissue site, with 3 acquisitions in a row, takes about one minute and leads to a set of 180 spectra (9 AF and 1 DR spectra acquired 3 times at 6 CEFS).

From a metrological point of view, rigorous calibration procedures are needed to ensure all measured results are meaningful when compared to each others between individuals or among time [22]. Table 2 summarizes the main calibration procedures performed on our programmable light source (including lamp, focusing lens, band-pass filters and excitation fibers of the probe) and on the detection channels (including sensing fibers of the probe, spectrograph's filter, diffraction grating and detector). The references of the corresponding calibration devices used for

#171682 - $15.00 USD Received 29 Jun 2012; revised 27 Sep 2012; accepted 28 Sep 2012; pub. 16 Nov 2012

TAB. 1. Acquisition parameters of the multichannel spectrometer with Gain = 1.7, ADC frequency = 20kHz and Slit width = 0.5mm, Output power was measured at the distal tip of the fiber probe

Measurements	Integration Time (ms)	Excitation Bands (nm)	Central peak Wavelength (nm)	Probe output Power (μW)	Emission Filters $\lambda_{cut-off}$ (nm)
AF	500	352-368	360	220	400
		362-378	370	123	
		372-388	380	115	435
		382-398	390	109	455
		392-408	400	120	
		402-418	410	120	
		412-428	420	101	475
		422-438	430	103	
		432-448	440	103	
DR	200	350-700	-	1540	no filter

each metrological configuration are given together with the frequency of application of these procedures (before each measure, daily, monthly). These calibration results served to correct raw spectra through a series of preprocessing steps detailed in the next section.

TAB. 2. Type of calibration measures performed for the experimental protocol with corresponding calibration devices and application frequencies

Calibration Type	Calibration device (references)	Frequency
Wavelength calibration of the spectrograph	HgAr Lamp (LSP035 HgAr Line Source, LOT)	monthly
Intensity response calibration	Calibrated Tungsten Lamp (DH-2000, Mikropack)	monthly
Background substraction	Shuttered light source	every 2 hours
Diffuse reflectance standard measurement	Integrating Sphere (ISP-30-6-IRRAD, Mikropack)	daily
Illumination energy normalization	Power meter (841-PE + 818-UV, Newport)	daily

2.3. Histo-Clinical Analysis

After spectra measurement, each tissue site was removed for histological analysis under conventional optical microscopy. The thicknesses of tissues' epidermis, dermis, perichondrium and cartilage were measured for every scar tissue. The dermal lymphocytes and fibroblasts densities were also examined for evaluating the cellular proliferation of underline tissue. Based on these measurements, two quantitative parameters were calculated to characterize the tissue samples : Dermal Fibroblasts Density (DFD) and Scar Elevation Index (SEI) [23]. SEI is a parameter related to the volume increase of tissue after scarring defined as the ratio between the scar elevation thickness ($h_{ss} - h_{ns}$) over the original thickness (h_{ns}) of the skin. DFD was measured by counting the number of fibroblasts per μm^2 in a tissue section. According to these criteria, all tissue samples were tagged as hypertrophic or non-hypertrophic by two experts. In short (please refer to [23] for details), mean dermal thickness, SEI and DFD are significantly higher in Hypertrophic scars (HT) than in Non-Hypertrophic scars (NHT) with p¡0.05 (Student's t-Test, n=25). The resulting classification (30 hypertrophic and 25 non-hypertrophic) was used as gold standard for developing our spectroscopic data-based classification algorithm. Examples of tissue slices and of rabbit'ear scars are given in Fig. 2.

#171682 - $15.00 USD Received 29 Jun 2012; revised 27 Sep 2012; accepted 28 Sep 2012; pub. 16 Nov 2012

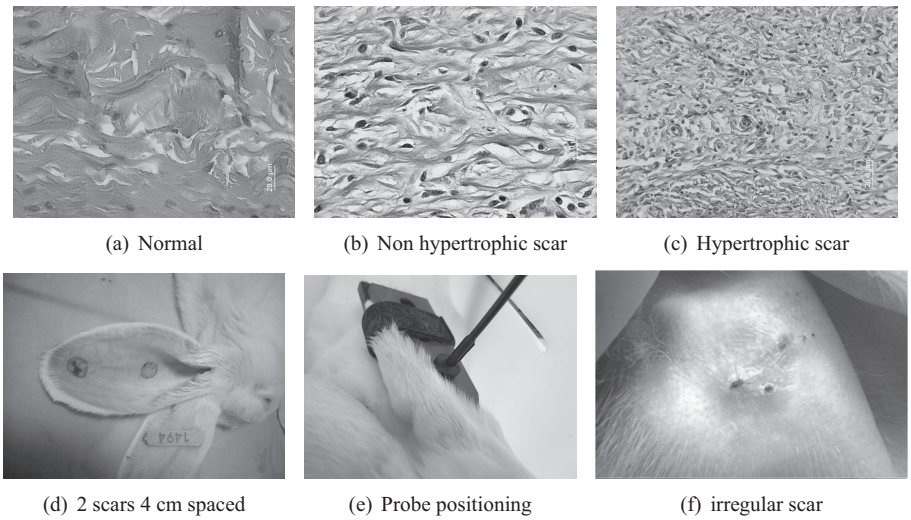

(a) Normal (b) Non hypertrophic scar (c) Hypertrophic scar

(d) 2 scars 4 cm spaced (e) Probe positioning (f) irregular scar

FIG. 2. (a), (b), (c) Images of histological slices for normal and scar tissues (Hematoxylin and Eosin stains). (d) scars on the ventral side of an anesthetized rabbit's ear. (e) fiber probe positioning piece. (f) irregular scar tissue (28 days after surgical wound)

3. Preprocessing of the raw spectra

Firstly, all acquired spectra were subtracted by a background spectrum measured at the same day with shuttered light source. Then, 3 subsequent spectra obtained under each configuration (every couple of excitation and CEFS) were averaged to obtain a higher SNR (Signal-to-Noise Ratio). A median filter with window frame size of 3 points (2.34*nm*) eliminated high amplitude narrow artifacts, while a Savitzky-Golay filter with window size of 25 points (20.25*nm*) eliminated high frequency noises by smoothing the spectra. Each intensity value of a AF spectrum was multiplied by a corresponding correction factor obtained by the spectral response calibration procedure (tungsten lamp). The spectrally corrected AF spectra were then normalized to the illumination power and exposure time for eliminating the influence of excitation intensity variations [22]. At last, all preprocessed spectra were normalized to their individual maximum for a line-shape analysis mentioned hereafter.

4. Spectroscopic Data Analysis

4.1. Initial selection of proper measurement sites

The strong light absorption due to erythema on some tissue sites deformed some acquired spectra to such an extent that they were not exploitable. Therefore, a revision algorithm eliminating all the data measured on these tissue sites was necessary before performing the spectral data classification. In general, these over-distorted spectra exhibiting quite different line-shape have intensity values non-correlated to those measured on most of tissue sites in the same class. Therefore, the median value of the inter-correlation vector of each spectrum was compared to a threshold (in our case 70%) so that a spectrum was considered as outlier if the value was less than the threshold i.e. eliminated from the data pool. By this method, we retained 44 (22 hypertrophic and 22 non-hypertrophic) out of 55 tissue sites for further analysis. The analysis of the tissue surface photographs and of the histological slice images confirmed the initial assumption that a very high blood level due to inflammatory reaction was found for most of these 11 eliminated sites.

#171682 - $15.00 USD Received 29 Jun 2012; revised 27 Sep 2012; accepted 28 Sep 2012; pub. 16 Nov 2012

4.2. *Feature extraction*

In order to extract discriminant features for classification, we first calculated the mean spectrum of each spectra class. The line-shapes of the class mean spectra represent the general spectral features in each class (intra-class spectra). The comparison of their line-shapes can help us to reveal discriminant features between spectra of different classes (inter-class spectra). A discriminant feature should be, for the most part, found in the spectral ranges where the intra-class spectra has more uniform intensity values and the inter-class ones differ the most. Here, intensity standard deviation (SD) was used to examine the intensity uniformity of the intra-class spectra. Fig. 3 shows the mean spectra and SD calculated for the normalized AF intensity spectra excited at 360*nm* and measured at the 5th CEFS (430μm). For both HT and NHT classes, the intensity spectra show a higher uniformity in the range between 400 and 680*nm* (SD $\in$ [0.016, 0.0519]). Hence, a threshold value of 0.05 was fixed for locating these "uniformity" ranges in all spectra acquired under different system configurations.

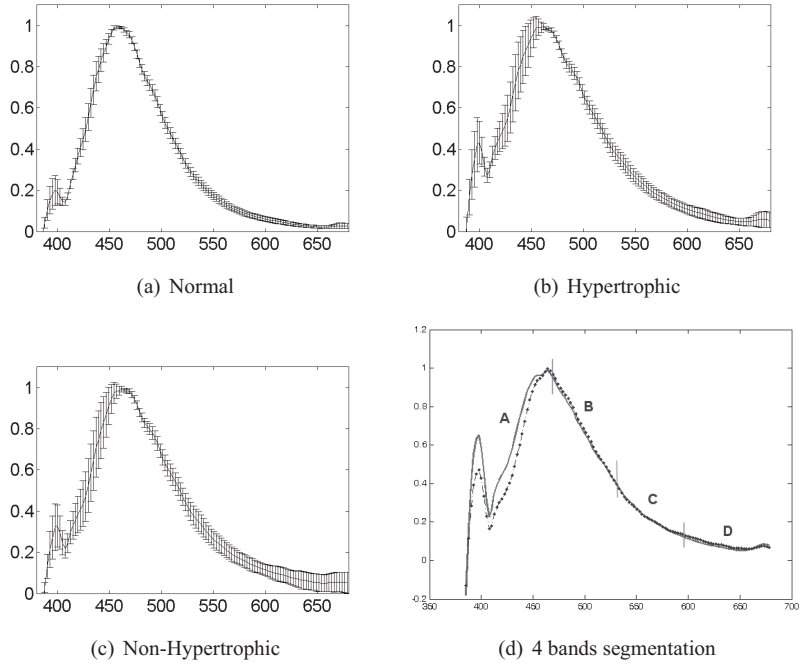

(a) Normal (b) Hypertrophic

(c) Non-Hypertrophic (d) 4 bands segmentation

FIG. 3. Mean±SD peak-normalized spectra excited at 368nm and measured at the CEFS of 438μm for (a) normal ($n = 22$), (b) hypertrophic scar (HT, $n = 22$) and (c) non-hypertrophic scar (NHT, $n = 22$) tissues. (d) Mean AF spectra for hypertrophic (bold line) and non-hypertrophic (dotted line) tissues excited at 368*nm* and measured at the 5th CEFS. The spectra are divided into 4 wavelength bands of 73nm width each (A :385-456nm, B :457-530nm, C :531-605nm, D :606-679nm) with respective correlation values : 0.943, 0.999, 0.999 and 0.866.

For locating the wavelength ranges where inter-class spectra (AF and RD) differ the most, another algorithm was developed based on the comparison of mean spectra correlations. Indeed, when two data sets are different, they must be independent and have relatively low correlation. Thus, we divided the class mean spectral curve into several pieces of equal size and analyzed locally their differences by calculating piece to piece their intensity correlation. As can be seen in Fig. 3, the ranges where the class mean spectra differ more from each other have low

#171682 - $15.00 USD Received 29 Jun 2012; revised 27 Sep 2012; accepted 28 Sep 2012; pub. 16 Nov 2012

correlation values (in the frames of A and D). On the other hand, the piece lengths defined for the correlation comparison can vary for revealing spectral differences at various scales. So, the mean spectra were segmented using various sizes (4 to 73 nm) and the piece to piece correlations were calculated at these different scales. A correlation threshold value of 0.95 was used to consider a wavelength range as "discriminant", and therefore of interest for carrying out the final feature extraction.

Interesting spectral features to be exploited can be either intensity absolute values or any other parameters representing the spectral line-shape like : mean intensities, under-curve areas, intensity or area ratios, slopes [18–20]. In a number of studies, statistical methods like Principle Component Analysis (ACP) have also been applied to the entire spectra in order to decompose the spectra into a linear combination of orthogonal basis (uncorrelated) spectra called Principal Components (PCs) [8, 24]. The first PC accounts for the spectral features that represents the most variation of the original data, and the subsequent ones represent features with progressively smaller variance. To describe a specific spectrum, a linear combination of PCs is used, with each PC weighted by the appropriate PC score. Typically, the value of these PC scores are used in classification but their complexity (linear combinations of numerous raw spectral intensities) is finally not easy to deal with, especially when it comes to the discussion on the signification of a limited exploitable number of intensity points.

The feature extraction implemented here addressed spectral features characterizing the line-shape of the normalized spectra of different tissues groups. Thus, the spectral slope was thought to be more interesting to exploit than other features and used alone as classification features. For calculating the slopes in each wavelength range, a linear least-square method was used to determine a line that has the best fit to the spectral curve spanning range. Finally, 486 slope characteristics in total were extracted from spectra (9AF + DF) measured for each scar site.

4.3. Feature selection

As presented in [25], though many candidate features are introduced to better represent the class domain due to unknown underlying class probabilities, the irrelevant and redundant features potentially present in the data set may affect the learning algorithm and reduce the classification performance. In addition, the large size of the 486-variables data set makes the classification problem more complicated, time-consuming, and yield a poor generalizing capability. A non-parametric significance statistical test (Mann-Whitney-Wilcoxon) was first applied to each feature, so as to examine whether its distribution was significantly independent for the two underlined classes. After this step, we obtain a subset of 112 features whose distribution was significantly independent for the different classes. Then, a heuristic method of stepwise regression was implemented for further feature selection. We started with a forward iterative selection procedure, during which variables were added one by one into the underline subset. The added feature remained in the subset if it enhanced the classification accuracy in terms of increasing the under-curve area in a Receiver Operating Characteristic (ROC). Otherwise, the feature was discarded. The iteration ended up when all features had been tested once. Afterward, the features in the resulting subset were discarded one by one, in order to examine if their abandoning would reduce the classification accuracy. If so, the discarded feature was included again in the subset, and otherwise definitely eliminated from the pool. At the end of these consecutive selection procedures, only 4 features were retained for the final classification (see Table 3).

#171682 - $15.00 USD Received 29 Jun 2012; revised 27 Sep 2012; accepted 28 Sep 2012; pub. 16 Nov 2012

TAB. 3. Set of the 4 selected slope features used for classification

CEFS (μm)	Excitation wavelength (nm)	AF emission wavelength bands (nm)	feature F
429	368	484 – 531	F1
438	410	528 – 599	F2
453	420	532.5 – 591.5	F3
672	410	626 – 648	F4

4.4. Supervised classification

The efficiency of a regularized linear classifier (Fisher's Linear Discriminant Analysis, LDA) and a non-regularized non-linear classifier (k-Nearest Neighbors, k-NN) were comparatively tested in the present study. Considering a linear combination of the characteristics, the first method aims at splitting the high-dimensional input space with a separation hyperplane. This separator is found by maximizing the ratio of between-class variance to the within-class variance. LDA can handle classification problems where the within-class frequencies are unequal and is well-regularized even when the data dimension is large such as in [19]. As for the k-NN, it provides non linear decision boundaries. It projects data of a test sample onto a multidimensional feature space consisting of the data from a labeled training set. The test sample is assigned with the most found class in its neighborhood including the k nearest training samples. This technique is simple and can deal with problems where data are totally confused. In addition, it can offer a good classification accuracy for low dimension problems which may be the case in our study, because the number of features was efficiently reduced in previous steps [18].

Leave-One-Out (LOO) cross-validation method [16, 19, 26] was performed to obtain unbiased classification results. In practice, one tissue site is excluded from the data set and k-NN (with k = 1) or LDA classifier is applied to the rest of this data set to generate a classifying scheme. The resulting scheme is then used to classify the previously excluded site. The classification result is compared to that obtained by the gold standard, such as histological analysis. We note 1 if the tissue site was correctly classified, and 0 otherwise. This process was repeated until all sites were excluded and tested once. The classification efficiency was asserted upon Sensibility (Se) and Specificity (Sp) calculated by the ratio of well classified to total tissue sites.Finally, we obtained the following results for each classifier : $Se = 85.7\%$ and $Sp = 94.4\%$ for LDA, $Se = 90.5\%$ and $Sp = 94.4\%$ for k-NN. The k-NN method gave the highest positive predictive and negative predictive values of 94.2% and 90.8% respectively.

5. Discussion

Looking at the final 4 most discriminant spectral features F1–F4 in Table 3, it can be noticed that none of them is relative to DR spectra. This observation implies the light absorption and diffusion due to chromophores (such as melanin and hemoglobin) do not contribute to the changes in DR spectra in a significantly enough way for differentiating between HT and NHT tissues. On the contrary, the absorption and scattering effects may partially contribute to discriminant changes in AF spectra. The curve-shape distortions of the *in vivo* AF spectra can be associated to changes in namely structural organization of the Extra-Cellular Matrix (ECM), blood volume, oxygen saturation of hemoglobin and mean depth of blood vessels and related to hypertrophic and non-hypertrophic cicatricial skin tissues. The 4 selected slopes are those of AF intensity spectra collected at excitation wavelengths 360, 410 and 420 nm, which puts forward their specific discrimination efficiency and also the relationship between hypertrophic tissues and the constitutive fluorophores excited at these wavelengths.

#171682 - $15.00 USD Received 29 Jun 2012; revised 27 Sep 2012; accepted 28 Sep 2012; pub. 16 Nov 2012

TAB. 4. AF emission wavelength peaks and bands reported in the literature for main skin endogenous fluorophores in epidermis and dermis (corresponding embedded layers in last row) excited at wavelengths 370, 410 and 420 nm.

Excitation	AF emission wavelength peaks and bands (*nm*)					
wavelength (*nm*)	NADH [4, 27, 28]	Flavins [4]	Porphyrins [4]	Collagen [27, 29]	Elastin [29, 30]	Keratin [28, 31, 32]
370	450-470	530-550		460	470	475
410	450-470	530-550	635, 670	490	480	
420	450-470	530-550	635, 670	490	480	500
Embedded place	cells	cells	cells	dermis	dermis	epidermis

Table 4 summarizes AF emission wavelength peaks and bands of the main skin fluorophores reported by previous studies using excitations around 370, 410 and 420*nm*. The epidermis is an avascular stratified squamous epithelium in which keratinocytes form the major proliferating cellular constituent. The dermis is a highly vascularized conjunctive layer in which assemble the collagen and elastin fibers into dense arrays [19, 20]. In hypertrophic skin, the tissue overgrowth is related to increased metabolic activity. Flavins and NADH, two major intra-cellular co-enzyme involved in metabolism mechanisms with emission peak respectively at 535*nm* and 460*nm*, are interesting for targeting this mechanism change [4, 27, 28]. Porphyrins are intermediate products in the cellular cycle characterized by two emission peaks at 635 and 670 nm [4]. Using spectral imaging to investigate the morphological structure changes in hypertrophic tissues, Chen et al. [21] found that collagen fiber network was disorganized and disrupted, resulting in a lower level of second harmonic generation signal on the fluorescent image. The distribution of elastin fibers was also disrupted but accumulated in a higher quantity in hypertrophic tissues thus generating more intense fluorescence. Collagen and elastin are structural proteins constituting the extracellular matrix in dermis. Their cross-links have a relatively high quantum efficiency compared with their monomers [37]. Cross-linking of fibrils is the origin of collagen fluorescence which emission peak (460 to 500*nm*) shifts with excitation (370 to 420*nm*). Same observation has been reported for elastin with emission peak shifts from 470 to 500*nm*.

When looking at the excitation-emission wavelength combinations relative to our discriminant features shown in Table 3, we could make some potential links between the information carried by :

- F1 and the biochemical changes in the epidermis (relative to keratin), in the dermis (elastin), and in both layers (flavins),
- F2 and F3 together, and changes relative to keratin in the epidermis, collagen in the dermis, and mainly flavins and lipopigments in both layers,
- F4 and the modifications associated to porphyrins in the epidermal and dermal cells.

It is worth noting that the 3 shortest feature-relative CEFS are close from each others (429, 438 and 453 *nm*). Indeed, for spatially resolved spectroscopy, using multiple collecting fibres at different CEFS can explore various tissue depths. For instance, it has been reported that using a CEFS of 250 μm allow excitations in the wavelength range $337-400nm$ arrive at depths of $225-250\mu m$ in skin tissues [33, 34]. [35] mentioned the maximum probing depth in an homogeneous medium (localized at $CEFS/2$) can be defined as $z_{max} = CEFS/2\sqrt{2}$. The Fig. 4 synthesizes the mean thickness ($\pm$SD)of epidermis and dermis measured for healthy, hypertrophic and non-hypertrophic samples, and the corresponding maximal exploring depths of our collecting probes defined by the aforementioned equation at feature-relative excitation wavelengths (below 420*nm*). It can be noticed that the 4 most discriminant features are obtained for the 4 firsts CEFS (429, 438, 453, 672 μm) among those tested here, offering a probing

#171682 - $15.00 USD Received 29 Jun 2012; revised 27 Sep 2012; accepted 28 Sep 2012; pub. 16 Nov 2012

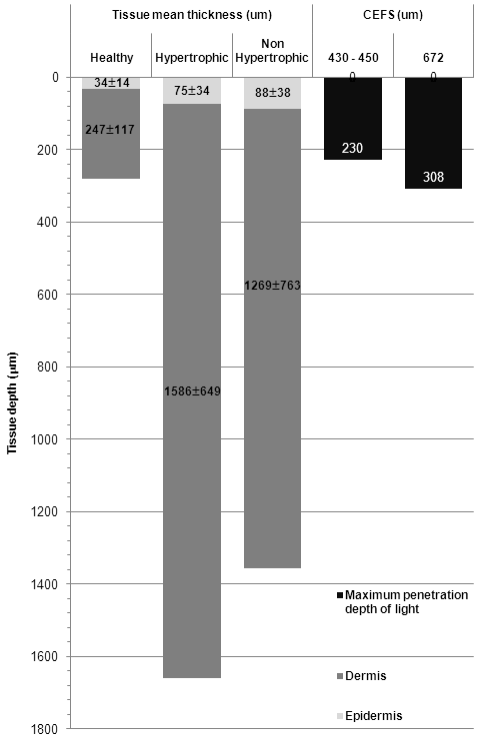

FIG. 4. Schematic representation of the correspondences between mean thicknesses measured for healthy, hypertrophic (HT) and non-hypertrophic (NHT) tissue samples and the maximum penetration depth of excitation lights below 420*nm* in relation with the two main discriminant CEFS 440 and 670μm

depth between 203 and 308μm (see Fig. 4). In this probing depth, dermis accounts for the major part in healthy tissue. However, during the scarring process, both epidermis and dermis thickness increases for hypertrophic and non-hypertrophic tissue. With this structural change, the exploring tissue portion changes and exhibits in the form of measured spectral line-shape, because fluorophores embedded in dermis give less and less contribution to the measured AF spectra.

The difference in fluorescence intensity between HT and NHT can also be reflected on the extracted features, though it is not as evident as on the images. This may be due to compensation of intensity contribution of two fluorophores excited (collagen and elastin) and emitting fluorescence in the same wavelength range [21]. Therefore, it could be interesting to test other spectral features, such as intensities ratio, for which the difference might be more pronounced. This could further enhance the classification performance. The obtained results corroborate the fact that morphological modifications in the matrix fiber network observed through a point spectroscopy modality may be a good tool to help the clinician for identifying scared skin tissue boundaries or for tracking skin scar formation.

6. Conclusion

In this study, the efficiency of bimodal (multi-AF and DR) spectroscopy was investigated in the detection of hypertrophic scar tissue on a preclinical model. A specific feature extraction and selection algorithm was developed and validated on our spectral data for classifying

#171682 - $15.00 USD Received 29 Jun 2012; revised 27 Sep 2012; accepted 28 Sep 2012; pub. 16 Nov 2012

hypertrophic and non-hypertrophic tissues, giving a sensibility of 90.5% and a specificity of 94.4%. Interpretation has been given relative to the discriminant features found by our extraction/selection methods. To our knowledge, this is the first use of spectroscopic methods on hypertrophic scar tissue. Considering this relative high diagnostic accuracy, our methods and findings can complete the future usage of spectroscopy in clinical dermatology.

Acknowledgment

The Authors express their grateful thanks to the regional committees (CD 52, 54) of the French "Ligue Contre le Cancer" for their financial support as well as the "Region Lorraine" and the Alexis Vautrin Cancer Center (CAV) for co-financing the PhD grant of H. Liu.

#171682 - $15.00 USD Received 29 Jun 2012; revised 27 Sep 2012; accepted 28 Sep 2012; pub. 16 Nov 2012